IOP Publishing Journal of Physics A: Mathematical and Theoretical
J. Phys. A: Math. Theor. **53** (2020) 154001 (28pp) https://doi.org/10.1088/1751-8121/ab79f2

Phase diagram of noisy systems of coupled oscillators with a bimodal frequency distribution

Alessandro Campa

National Center for Radiation Protection and Computational Physics, Istituto Superiore di Sanità, Viale Regina Elena 299, 00161 Rome, Italy

E-mail: alessandro.campa@iss.it

Received 2 August 2019, revised 6 February 2020
Accepted for publication 25 February 2020
Published 23 March 2020

Abstract

We study the properties of large systems of globally coupled oscillators in the presence of noise. When the distribution of the natural frequencies of the oscillators is bimodal and its analytical continuation in the complex plane has only a few poles in the lower half plane, the dynamics of the system, governed by a Fokker–Planck equation for the single particle distribution function, can be reduced to a system of ordinary differential equations describing the dynamics of suitably defined order parameters, the first ones of which are related to the usual synchronization order parameter. We obtain the full phase diagram of the oscillator system, that shows a very rich behaviour, with regions characterized by synchronized states, regions with periodic states, and others with bi-stability, associated to the presence of hysteresis. The latter phenomenon is confirmed by numerical simulations ot the full system of coupled oscillators. We compare our results with those previously obtained for noiseless systems, and we show that for increasing noise the phase diagram changes qualitatively, tending to the simple diagram that is found for systems with unimodal frequency distributions.

Keywords: synchronization transition, phase diagram, bi-stability, hysteresis

1. Introduction

The phenomenon of collective synchronization in systems made of a large population of coupled oscillatory units is now recognized as a very important subject of investigation, since it is naturally found in many different situations [1]. Although the units are characterized by different natural frequencies, they can spontaneously synchronize and oscillate at a common

frequency. This cooperative effect can be found in physical and biological systems, like flashing in unison by groups of fireflies [2], voltage oscillations at a common frequency in an array of current-biased Josephson junctions [3], synchronized firings of cardiac pacemaker cells [4], metabolic synchrony in yeast cell suspensions [5], phase synchronization in electrical power distribution networks [6], animal flocking behaviour [7]. A survey of the examples occurring in nature is in [8].

It is not possible to overestimate the great importance of the introduction of the Kuramoto model for the theoretical study of synchronization in systems of interacting oscillators [9, 10]. The model makes several assumptions; in particular, it assumes that the oscillators are represented by a single dynamical variable, the phase, and that the coupling strength K is the same between all pairs of oscillators; besides, the interaction is very simple, depending only on the sine of the phase difference of the pair. In spite of these simplifying characteristics, the model captures the essential physics of the dynamics, in which the interaction can induce a macroscopic fraction of the oscillators, each one with a proper frequency drawn from a given distribution $g(\omega)$, to spontaneously synchronize.

The original model has been extended along several directions. In the Kuramoto model the proper frequencies of the oscillators are quenched variables. However, the recognition of the fact that the natural frequency of each oscillatory unit can fluctuate for various reasons (we remind that the simple phase representation can model in an effective way a quite complex physical or biological unit), has led to the introduction of noise in the dynamics, transforming the original deterministic equations in Langevin equations [11]. This noise can be thought of as mimicking the effect of frequency fluctuations; thus the strength of the noise is directly related to the amplitude of these fluctuations. Another generalization has been the introduction of inertia, proposed as a way to improve the modelization of the approach to synchronization [12]. Taken together, the two generalizations result in a second-order dynamical system subject to noise [13, 14].

A prominent role is played by the frequency distribution function $g(\omega)$. Most of the reasearch has been devoted to the case of a unimodal distribution, i.e., to the case where $g(\omega)$ has a unique maximum at a frequency $\omega = \omega_0$, around which it is symmetrical, decaying monotonically to zero for increasing $|\omega - \omega_0|$. In this case the Kuramoto model has a synchronization transition at the value $K_c = \frac{2}{\pi g(\omega_0)}$ of the coupling; for smaller values the oscillators do not synchronize and each one oscillates with its own proper frequency, while for $K > K_c$ a fraction of the oscillators synchronize at $\omega = \omega_0$, the fraction increasing continuosly for increasing K, from 0 at K_c to 1 when K becomes very large (formally for $K \to \infty$) [15]. This picture holds for the model augmented with noise, although the threshold value for K depends on the noise strength [11, 16]. However, for more general frequency distributions, the overall scenario can be more complex, as shown by, e.g., numerical simulations of the dynamics when $g(\omega)$ is bimodal, having two equal maxima at two different frequencies [17]: the system of oscillators can present bi-stability and also seemingly periodic asymptotic states.

Independently from the role played by the distribution $g(\omega)$ in determining the possible synchronized states of the system of oscillators, another problem, in a theoretical analysis, is represented by the study of the dynamics itself. As shown in the next section, the dynamics can be described, at least in the limit of a very large number of oscillators (formally, for $N \to \infty$), by a system of coupled nonlinear Fokker–Planck equations for the time dependent single particle distribution function. As will be clear, the asymptotic stationary distributions at large times are related, when different from a homogeneous distribution, to the synchronized states. However, the analysis of the full dynamics as determined by this system of Fokker–Planck equations is not a trivial task, and it is much more feasible to find its possible stationary states

and the behaviour of the system, perturbatively, when the coupling K is near the critical value K_c [15, 17]. In fact, it has to be considered that this time evolution occurs in a space characterized by a double continuous infinity: that of the oscillator phase variable and that of the proper frequency ω. The former can be trasformed to a countable infinity by going to Fourier space and obtaining an infinite set of equations for each ω, the systems being coupled (this will appear clearly in the next section); however, this does not imply a real simplification of the problem.

In this respect, a breakthrough has been provided, in the study of noiseless systems, by the Ott–Antonsen ansatz [18], that allows to reduce the dynamics to that of a single Fourier component of the single particle distribution. However, the problem is still infinite dimensional, to account for the dependence on ω: the single Fourier component depends not only on time, but also on ω. But the reduction goes further if the frequency distribution function $g(\omega)$ can be analytically continued in the complex plane and this continuation has only few poles in the lower half plane; then, it is possible to study directly the full dynamics of few variables (practically, two real equations for each pole of the analytical continuation) that are simply related to the synchronization of the system; this will be completely clear in the next section. One has a low-dimensional system of ordinary differential equations.

While this approach has confirmed the picture previously described for unimodal distributions $g(\omega)$, its application to a bimodal $g(\omega)$, with two poles in the lower half complex plane, has revealed the great richness of the possible states of the system of noiseless oscillators [19]. In this latter work, the results have been obtained by the study of a system of four ordinary differential equations, reduced to two by simple and plausible physical arguments. The analysis of a twodimensional dynamical system has made it possible to obtain a full phase diagram of the asymptotic states. Unfortunately, the introduction of noise prevents the use of the Ott–Antonsen ansatz, as will be shown.

The main purpose of this paper is to show that, with frequency distributions $g(\omega)$ that, when analitically continued, enjoy the above mentioned property of having few poles in the lower half of the complex plane, a reduction of the dynamics and the determination of the phase diagram are still possible, in spite of the impossibility to introduce the Ott–Antonsen ansatz. More precisely, while it is not possible to reduce the infinite dimensionality due to the dependence on the oscillator phase, we can eliminate the infinite dimensionality deriving from the dependence on the proper frequency ω. One is then left with a system of ordinary differential equations that do not depend any more on ω. From the computational point of view, it is important to stress that, even if in principle the system is made of an infinite number of equations, it is possible to restrict the analysis to a truncated system of few tens of equations. To summarize, the starting double continuous infinity is reduced, in principle, to a simple countable infinity, and in practice to a system of few tens of ordinary differential equations, readily accessible by numerical investigation.

Operatively, we will consider the possible synchronized states, and the periodic asymptotic states, of a noisy system of coupled oscillators, in which the frequency distribution $g(\omega)$ is bimodal and has two poles in the lower half of the complex plane. Although the number of equations is not equal to 2 as for the noiseless system where the Ott–Antonsen ansatz can be introduced, and then an almost complete analytical study of the solutions is not affordable, the system can be very rapidly analyzed numerically, and in particular also the stability of synchronized states can be studied, something that is extremely difficult for the full Fokker–Planck equation. The detailed phase diagram, showing all the possible asymptotic states of the system, can be obtained.

Recently a procedure has been developed for the analysis of systems where the Ott–Antonsen ansatz is not valid [20–22]; for a frequency distribution $g(\omega)$ with the properties

cited above, also this procedure allows to reduce the problem to a set of ordinary differential equations. In specific points of the paper we will refer to this other method to make a connection with the results presented here, and more extended comments will be made in the conclusions.

The structure of the paper is as follows. In section 2 we introduce the model and we derive the system of equations. In section 3 we study the stationary states and their stability, while in section 4 we focus on the periodic asymptotic states; in these two sections, we concentrate on a given value of the noise strength, and we present the full phase diagram (in the parameter space) of the system, that interestingly includes regions of bi-stability; besides, we make a brief analysis of the bifurcations associated to the transitions from one stationary state to another (or from a stationary state to a periodic state). In section 5 we consider the phase diagram at increasingly larger noise strength, showing how the diagram simplifies, approaching the one valid for a unimodal distribution. In section 6 we compare the results of our analysis with those of a numerical simulation of the full system of noisy coupled oscillators. Besides showing the agreement of the two evaluations, the section focuses to the presence of hysteresis in the dynamics, directly associated to the presence of bi-stability regions in the phase diagram. Section 7 presents a discussion and draws some conclusions.

2. Derivation of the system of equations

The Langevin equations describing the dynamics of N oscillators that interact with a coupling as in the Kuramoto model, are [11]:

$$\frac{\mathrm{d}\theta_i}{\mathrm{d}t} = \omega_i - \frac{K}{N}\sum_{j=1}^{N} \sin\left(\theta_i - \theta_j\right) + \eta_i(t), \quad i = 1, \ldots, N, \tag{1}$$

where $\theta_i \in [0, 2\pi)$ is the phase of the ith oscillator, ω_i is its natural frequency, and K is the coupling constant. The stochastic noise $\eta_i(t)$ is independent from those of the other oscillators, and each $\eta_i(t)$ is Gaussian distributed at each time, while the noises at different times are uncorrelated. Then we have the expectation values (averaging over noise realizations):

$$\langle \eta_i(t) \rangle = 0\,, \quad \langle \eta_i(t)\eta_j(t') \rangle = 2D\delta_{ij}\delta(t - t'), \tag{2}$$

where the coefficient D characterizes the noise intensity. The natural frequencies ω_i are distributed according to a given frequency distribution function $g(\omega)$. As anticipated above, we will treat the case of a symmetric bimodal frequency distribution, given in particular by the sum of two Lorentzians of width Δ, one centered in $\omega = \omega_0$ and one in $\omega = -\omega_0$:

$$g(\omega) = \frac{\Delta}{2\pi}\left[\frac{1}{(\omega - \omega_0)^2 + \Delta^2} + \frac{1}{(\omega + \omega_0)^2 + \Delta^2}\right], \tag{3}$$

which is normalized, $\int_{-\infty}^{+\infty} \mathrm{d}\omega\, g(\omega) = 1$. It is actually bimodal only if $\omega_0 > \frac{\Delta}{\sqrt{3}}$. If this condition is not satisfied, $g(\omega)$ is symmetric and unimodal, in which case the known results [15, 16] do not show the richness of different behaviours that is found for bimodal distributions[1].

[1] We remind that usually one considers frequency distributions centered in $\omega = 0$. This is not a loss of generality, since with a distribution centered at any given value ω^*, it is possible to perform a change of variables $\theta_i \to \theta_i + \omega^* t$, going back to the former case.

In the $N \to \infty$ limit the dynamics can be described by the following Fokker–Planck equation for the single particle distribution function $\rho(\theta, \omega, t)$:

$$\frac{\partial}{\partial t}\rho(\theta,\omega,t) = -\frac{\partial}{\partial \theta}\left[(\omega + F(\theta,t))\,\rho(\theta,\omega,t)\right] + D\frac{\partial^2}{\partial \theta^2}\rho(\theta,\omega,t), \tag{4}$$

where $\rho(\theta, \omega, t)\mathrm{d}\theta\mathrm{d}\omega$ gives the fraction of oscillators with natural frequencies in the range $(\omega, \omega + \mathrm{d}\omega)$ that at time t have phases in the range $(\theta, \theta + \mathrm{d}\theta)$. The distribution $\rho(\theta, \omega, t)$ is normalized for each ω, i.e., $\int_0^{2\pi} \mathrm{d}\theta\, \rho(\theta, \omega, t) = 1$, normalization which is conserved by the Fokker–Planck equation. We see that actually equation (4) is a system of partial differential equations, one for each ω, which are coupled by the force term $F(\theta, t)$, given by

$$F(\theta,t) = K\int_{-\infty}^{+\infty}\mathrm{d}\omega\int_0^{2\pi}\mathrm{d}\theta' g(\omega)\sin(\theta'-\theta)\rho(\theta',\omega,t). \tag{5}$$

It is important to realize that equation (4) is a nonlinear equation, since the force term $F(\theta, t)$ depends on the distribution $\rho(\theta, \omega, t)$ itself, as shown in equation (5). The degree of synchronization of the system is best described by the complex order parameter $r(t)$, defined by

$$r(t) = \int_{-\infty}^{+\infty}\mathrm{d}\omega\int_0^{2\pi}\mathrm{d}\theta g(\omega)\mathrm{e}^{\mathrm{i}\theta}\rho(\theta,\omega,t). \tag{6}$$

From equations (5) and (6) we see that $F(\theta, t) = K\ \mathrm{Im}\left[r(t)\mathrm{e}^{-\mathrm{i}\theta}\right]$. The order parameter satisfies $|r(t)| \leqslant 1$. In an incoherent state we have $|r| = 0$, while a fully synchronized state has $|r| = 1$. Using the order parameter in the Fokker–Planck equation (4), we obtain the expression which is useful for the following analysis:

$$\frac{\partial}{\partial t}\rho(\theta,\omega,t) = -\frac{\partial}{\partial \theta}\left[\left(\omega + \frac{K}{2\mathrm{i}}(r(t)\mathrm{e}^{-\mathrm{i}\theta} - r^*(t)\mathrm{e}^{\mathrm{i}\theta})\right)\rho(\theta,\omega,t)\right] + D\frac{\partial^2}{\partial \theta^2}\rho(\theta,\omega,t), \tag{7}$$

where, as usual, the star denotes complex conjugation. A Fourier expansion of the distribution function gives:

$$\rho(\theta,\omega,t) = \frac{1}{2\pi}\sum_{n=-\infty}^{+\infty} f_n(\omega,t)\mathrm{e}^{\mathrm{i}n\theta}. \tag{8}$$

The normalization and the reality of $\rho(\theta, \omega, t)$ imply that $f_0(\omega, t) \equiv 1$ and $f_{-n}(\omega, t) = f_n^*(\omega, t)$. Substituting the Fourier expansion in the Fokker–Planck equation (7) we obtain the following system of differential equations:

$$\begin{aligned}\dot{f}_n(\omega,t) \equiv \frac{\partial f_n(\omega,t)}{\partial t} &= -\mathrm{i}n\omega f_n(\omega,t)\\ &\quad - \frac{K}{2}n\left[r(t)f_{n+1}(\omega,t) - r^*(t)f_{n-1}(\omega,t)\right] - Dn^2 f_n(\omega,t).\end{aligned} \tag{9}$$

We see that the equation for $n = 0$ gives $\dot{f}_0 = 0$, coherently with the fact that $f_0 \equiv 1$, and that the two open subsystems for $n > 0$ and $n < 0$ are decoupled; however, the subsystem for $n < 0$ is simply the complex conjugate of that for $n > 0$, since $f_{-n} = f_n^*$, and it is not necessary to consider it.

When $D = 0$, the Ott–Antonsen ansatz consists in assuming that $f_n(\omega, t) = f_1^n(\omega, t)$ for each n [18, 19]. One of the physical justification for the ansatz is that the known forms of the stationary states of the Kuramoto model, both for the incoherent and for the synchronized case, satisfy the ansatz. It is easy to see that, plugging the ansatz in each one of the equations (9), they all become equal to the equation for $f_1(\omega, t)$. The presence of the noise term, i.e. the last term of each equation of the system, does not allow to make the ansatz; this is also consistent with the fact that the stationary solution of equation (7) does not satisfy it [11, 16]. However, as we will show, in spite of this, the frequency distribution (3) makes it possible to perform an analysis of the dynamics of the order parameter (6), and to obtain a full phase diagram. As it will be clear in the following, this analysis is possible when the frequency distribution can be analytically continued in the complex ω plane and it vanishes in the whole lower half plane when $|\omega| \to \infty$; this is not verified, e.g., for a Gaussian frequency distribution. It will also be clear that the analysis is practically feasible when the number of poles of the distribution is small.

After having obtained, for $D = 0$, a closed equation for $f_1(\omega, t)$, in the successive analysis it is assumed that $f_1(\omega, t)$ has no singularities in the lower half plane, and that $f_1(\omega, t) \to 0$ for $\mathrm{Im}(\omega) \to -\infty$, the latter being based on the fact that it holds for any $t > 0$ if it holds for $t = 0$ [19]. In our case we have to keep all the Fourier terms f_n, and we make the analogous assumptions that $f_n(\omega, t)$ do not have singularities in the lower half plane and that $f_n(\omega, t) \to 0$ for $\mathrm{Im}(\omega) \to -\infty$. These assumptions can be justified as follows. We first note that the system of equations (9) can be continued to the complex ω plane[2]. Second, denoting a complex ω with $\omega_\mathrm{R} + \mathrm{i}\omega_\mathrm{I}$, for large negative ω_I the equation for f_n can be approximated with $\dot{f}_n(\omega, t) = -|\omega_\mathrm{I}| f_n(\omega, t)$, showing that for $t > 0$ we have $f_n(\omega, t) \to 0$ when $\omega_\mathrm{I} \to -\infty$, if this holds for $t = 0$.

Since we have to study the whole system of equations for positive n, it is useful to use the generalized complex order parameters

$$r_n(t) = \int_{-\infty}^{+\infty} \mathrm{d}\omega \int_0^{2\pi} \mathrm{d}\theta g(\omega) \mathrm{e}^{\mathrm{i}n\theta} \rho(\theta, \omega, t). \tag{10}$$

These order parameters were introduced by Daido for a detailed study of the synchronization transition in the extension of the Kuramoto model made of a (noiseless) system of coupled oscillators in which the interaction between each pair of oscillators is a generic function of their phase difference [23–26]. We see that the usual order parameter $r(t)$ is given by $r_1(t)$. Substituing the Fourier expansion for $\rho(\theta, \omega, t)$ we find

$$r_n(t) = \int_{-\infty}^{+\infty} \mathrm{d}\omega \, g(\omega) f_{-n}(\omega, t), \tag{11}$$

or analogously

$$r_n^*(t) = \int_{-\infty}^{+\infty} \mathrm{d}\omega \, g(\omega) f_n(\omega, t), \tag{12}$$

[2] If we consider the system for complex ω, then it is no more true that the equations for negative n are the complex conjugates of those for positive n, and in fact for complex ω we cannot consider anymore $\rho(\theta, \omega, t)$ to be real, and that $f_{-n} = f_n^*$. However, this is not relevant, since, as we have seen, the subsysytems for negative and positive n are decoupled, and for our analysis of the dynamics of the order parameter (6) we need only the equations with positive n.

At this point one can make use of the above properties of the frequency distribution $g(\omega)$. Suppose that this function has q poles in the lower half plane, denoted by $\omega_1, \ldots, \omega_q$, and that it vanishes, in this half plane, when $|\omega| \to \infty$. Then, from equation (12) we obtain

$$r_n^*(t) = -2\pi \mathrm{i} \sum_{s=1}^{q} \mathrm{Res}\left[g(\omega) f_n(\omega, t)\right]\big|_{\omega=\omega_s}, \tag{13}$$

i.e., $r_n^*(t)$ is proportional to the sum of the residues of the function $g(\omega) f_n(\omega, t)$ computed at the poles of $g(\omega)$. The poles in the lower half plane of the function $g(\omega)$ in equation (3) are in $\omega = \omega_0 - \mathrm{i}\Delta$ and in $\omega = -\omega_0 - \mathrm{i}\Delta$, and are simple. Then, from equation (13) we get

$$r_n^*(t) = \frac{1}{2} f_n(\omega_0 - \mathrm{i}\Delta, t) + \frac{1}{2} f_n(-\omega_0 - \mathrm{i}\Delta, t). \tag{14}$$

At this point we can define

$$r_n^{(1)*}(t) = f_n(\omega_0 - \mathrm{i}\Delta, t) \tag{15}$$

$$r_n^{(2)*}(t) = f_n(-\omega_0 - \mathrm{i}\Delta, t), \tag{16}$$

so that

$$r_n(t) = \frac{1}{2}\left[r_n^{(1)}(t) + r_n^{(2)}(t)\right] \tag{17}$$

From the equations (9) we thus have:

$$\dot{r}_n^{(1)*} = -n\left(\Delta + \mathrm{i}\omega_0 + nD\right) r_n^{(1)*} - \frac{K}{4} n \left[\left(r_1^{(1)} + r_1^{(2)}\right) r_{n+1}^{(1)*} - \left(r_1^{(1)*} + r_1^{(2)*}\right) r_{n-1}^{(1)*}\right] \tag{18}$$

$$\dot{r}_n^{(2)*} = -n\left(\Delta - \mathrm{i}\omega_0 + nD\right) r_n^{(2)*} - \frac{K}{4} n \left[\left(r_1^{(1)} + r_1^{(2)}\right) r_{n+1}^{(2)*} - \left(r_1^{(1)*} + r_1^{(2)*}\right) r_{n-1}^{(2)*}\right], \tag{19}$$

i.e.,

$$\dot{r}_n^{(1)} = -n\left(\Delta - \mathrm{i}\omega_0 + nD\right) r_n^{(1)} - \frac{K}{4} n \left[\left(r_1^{(1)*} + r_1^{(2)*}\right) r_{n+1}^{(1)} - \left(r_1^{(1)} + r_1^{(2)}\right) r_{n-1}^{(1)}\right] \tag{20}$$

$$\dot{r}_n^{(2)} = -n\left(\Delta + \mathrm{i}\omega_0 + nD\right) r_n^{(2)} - \frac{K}{4} n \left[\left(r_1^{(1)*} + r_1^{(2)*}\right) r_{n+1}^{(2)} - \left(r_1^{(1)} + r_1^{(2)}\right) r_{n-1}^{(2)}\right]. \tag{21}$$

Equations (20) and (21), for $n = 1, 2, \ldots$, or better their dimensionless version to be introduced shortly, are the basic equations of our study. In the equation for $n = 1$ there appear $r_0^{(1)}$ and $r_0^{(2)}$, that are understood to be identically equal to 1. We see that from the original Fokker–Planck equation (7), where we had an infinite dimensional dynamical system labelled by two continuous variables θ and ω, we have obtained a dynamical system which is still infinite dimensional, but labelled by only the discrete variable n. This has been made possible

by the above mentioned properties of the frequency distribution $g(\omega)$, and it is due to the fact that we restrict our interest on the dynamics of the order parameters. We emphasize here two things: the order parameters, and in particular r_1, are the most relevant quantities in our system of interacting oscillators, on which the characterization of the properties of the asymptotic states are based. Second, we repeat that without the above properties of $g(\omega)$ one could not go beyond equation (9), so that a system of discrete differential equations for the order parameters could not be written[3].

The approach introduced in [20–22], if applied to our case of a frequency distribution given by the sum of two Lorentzians, would make use of different dynamical variables, that however can be expressed in terms of $r_n^{(1)}$ and $r_n^{(2)}$, obtaining another system of differential equations. We come back to this point in section 2.2, after showing what happens to our system in the noiseless case.

2.1. Reduced variables

The system can conveniently be studied using dimensionless parameters; this also allows an easier comparison with the results of the noiseless ($D = 0$) system [19]. This can be achieved by defining the quantities $\widehat{\Delta} = \frac{4}{K}\Delta$, $\widehat{\omega}_0 = \frac{4}{K}\omega_0$, $\widehat{D} = \frac{4}{K}D$, and $\widehat{t} = \frac{K}{4}t$. Equations (20) and (21) now read

$$\dot{r}_n^{(1)} = -n\left(\widehat{\Delta} - \mathrm{i}\widehat{\omega}_0 + n\widehat{D}\right) r_n^{(1)} - n\left[\left(r_1^{(1)*} + r_1^{(2)*}\right) r_{n+1}^{(1)} - \left(r_1^{(1)} + r_1^{(2)}\right) r_{n-1}^{(1)}\right] \tag{22}$$

$$\dot{r}_n^{(2)} = -n\left(\widehat{\Delta} + \mathrm{i}\widehat{\omega}_0 + n\widehat{D}\right) r_n^{(2)} - n\left[\left(r_1^{(1)*} + r_1^{(2)*}\right) r_{n+1}^{(2)} - \left(r_1^{(1)} + r_1^{(2)}\right) r_{n-1}^{(2)}\right], \tag{23}$$

where now the dot denotes differentiation with respect to $\widehat{t}$. In the following, to ease the notation we will drop the hat over the dimensionless parameters. Only in section 6, presenting the results of numerical simulations of the full system of equations (1), we will reintroduce the use of the hat, since we will have to refer also to the original system parameters.

We are interested in the asymptotic solutions of the system of equations. As we will see, these are given either by stable stationary states, or by standing wave states. We note that the equations are invariant with respect to the transformation $r_n^{(1)} \to r_n^{(1)}\mathrm{e}^{-\mathrm{i}n\psi}$ and $r_n^{(2)} \to r_n^{(2)}\mathrm{e}^{-\mathrm{i}n\psi}$ for arbitrary ψ; this is a consequence of the global rotational invariance of the system.

2.2. The noiseless case

For completeness we show what happens when $D = 0$. The above equations in the reduced variables for the evolution of $r_n^{(1)}$ and $r_n^{(2)}$ become

$$\dot{r}_n^{(1)} = -n\left(\Delta - \mathrm{i}\omega_0\right) r_n^{(1)} - n\left[\left(r_1^{(1)*} + r_1^{(2)*}\right) r_{n+1}^{(1)} - \left(r_1^{(1)} + r_1^{(2)}\right) r_{n-1}^{(1)}\right] \tag{24}$$

$$\dot{r}_n^{(2)} = -n\left(\Delta + \mathrm{i}\omega_0\right) r_n^{(2)} - n\left[\left(r_1^{(1)*} + r_1^{(2)*}\right) r_{n+1}^{(2)} - \left(r_1^{(1)} + r_1^{(2)}\right) r_{n-1}^{(2)}\right]. \tag{25}$$

[3] For general $g(\omega)$ it is possible to write a system of linear differential equations, system labelled by the continuous variable ω, that can be solved with the Laplace transform, but this analysis is restricted to the study of the dynamics of a vanishingly small order parameter $r_1(t)$, i.e., to the stability analysis of the incoherent state $r_1 = 0$ [15].

As we have remarked in the preceding Section, the Ott–Antonsen ansatz is the assumption that $f_n(\omega,t) = f_1^n(\omega,t)$ for each n, where $f_n(\omega,t)$ is the nth Fourier coefficient in (8). Looking at equations (15) and (16), it is clear that this implies that $r_n^{(1)}(t) = \left[r_1^{(1)}(t)\right]^n$ and $r_n^{(2)}(t) = \left[r_1^{(2)}(t)\right]^n$. Inserting these equalities in equations (24) and (25), it is easily seen that for each n the equations are identical to those for $n = 1$, i.e.

$$\dot{r}_1^{(1)} = -(\Delta - \mathrm{i}\omega_0)\, r_1^{(1)} - \left[\left(r_1^{(1)*} + r_1^{(2)*}\right)\left[r_1^{(1)}\right]^2 - \left(r_1^{(1)} + r_1^{(2)}\right)\right] \tag{26}$$

$$\dot{r}_1^{(2)} = -(\Delta + \mathrm{i}\omega_0)\, r_1^{(2)} - \left[\left(r_1^{(1)*} + r_1^{(2)*}\right)\left[r_1^{(2)}\right]^2 - \left(r_1^{(1)} + r_1^{(2)}\right)\right] \tag{27}$$

(recalling that $r_0^{(1)}$ and $r_0^{(2)}$ are identically equal to 1). Thus, the dynamics of the system is reduced to that of a couple of (complex) ordinary differential equations. This reduction also shows that the initial assumption is conserved by the dynamics, namely, the manifold, in the distribution function space, defined by the Ott–Antonsen ansatz, is invariant [18]. It does not prove, however, that any initial distribution outside the manifold is attracted towards the manifold by the dynamics, although the numerical solution of the equations shows that this actually happens.

Considering now again the general case with positive D, dynamical variables $\varkappa_n^{(1)}$ and $\varkappa_n^{(2)}$, analogous to those introduced in [20–22] and denoted as circular cumulants, can be expressed in terms of our variables by using a cumulant-generating function, and they can be particularly useful when the noise D is small. While details can be found in the cited references, an idea is obtained by saying that in our case the circular cumulants for $n = 1$, i.e., $\varkappa_1^{(1)}$ and $\varkappa_1^{(2)}$, would be identical, respectively, to $r_1^{(1)}$ and $r_1^{(2)}$, but for $n = 2$ they would be given by $\varkappa_2^{(j)} = r_2^{(j)} - \left[r_1^{(j)}\right]^2$ $(j = 1, 2)$. From this definition it is clear that in the manifold defined by the Ott–Antonsen ansatz, a manifold that as we have seen is invariant when $D = 0$, one has $\varkappa_2^{(j)} \equiv 0$. The same can be seen to occur for all the circular cumulants for $n > 2$. Then, it is to be expected that at low noise the dynamical variables $\varkappa_n^{(j)}(t)$ for $n \geqslant 2$ are small.

3. The stationary states

3.1. The incoherent state and its stability

For any value of the parameters, the incoherent state $r_n^{(1)} = r_n^{(2)} = 0$ for any n is a solution of the system of equations. We begin our analysis by studying the stability of the incoherent solution. By linearizing equations (22) and (23) we obtain:

$$\dot{r}_1^{(1)} = -(\Delta - \mathrm{i}\omega_0 + D)\, r_1^{(1)} + (r_1^{(1)} + r_1^{(2)}) \tag{28}$$

$$\dot{r}_1^{(2)} = -(\Delta + \mathrm{i}\omega_0 + D)\, r_1^{(2)} + (r_1^{(1)} + r_1^{(2)}) \tag{29}$$

$$\dot{r}_n^{(1)} = -n\,(\Delta - \mathrm{i}\omega_0 + nD)\, r_n^{(1)} \quad n > 1 \tag{30}$$

$$\dot{r}_n^{(2)} = -n\,(\Delta + \mathrm{i}\omega_0 + nD)\, r_n^{(2)} \quad n > 1, \tag{31}$$

The incoherent state is stable when all the eigenvalues of this linear system have a negative real part. The equations for $n > 1$ are all decoupled, and they directly give the eigenvalues,

all of which with negative real part equal to $-n\Delta - n^2 D$. The two equations for $n = 1$, on the other hand, are coupled, and a simple calculation shows that the corresponding eigenvalues are given by:

$$\lambda_{\pm} = -(\Delta + D - 1) \pm \sqrt{1 - \omega_0^2} \tag{32}$$

The phase diagram will be considered, for any given fixed value of D, in the first quadrant of the (ω_0, Δ) plane (more precisely, the region of the plane defined by $\omega_0 \geqslant 0$ and $\Delta > 0$, which is the meaningful case). Then, let us see which are, in this quadrant, the boundaries defining the regions where the incoherent state is stable. This occurs when the real part of the right hand side of equation (32) is negative for both λ_+ and λ_-. We have to distinguish the cases $\omega_0 \leqslant 1$ and $\omega_0 > 1$. In the former case λ_+ and λ_- are real, with $\lambda_+ \geqslant \lambda_-$ (equality holds for $\omega_0 = 1$); in the latter case λ_+ and λ_- are complex conjugate. Thus, for $\omega_0 \leqslant 1$ stability requires that $\lambda_+ < 0$, i.e., $\Delta > 1 - D + \sqrt{1 - \omega_0^2}$. This inequality defines, in the first quadrant of the (ω_0, Δ) plane, the part of the strip $0 \leqslant \omega_0 \leqslant 1$ which is above the circumference with center in $(\omega_0, \Delta) = (0, 1 - D)$ and radius equal to 1. We note that when $D \geqslant 2$ this region coincides with the entire strip. On the other hand, for $\omega_0 > 1$ the condition for stability is $\mathrm{Re}\,[\lambda_{\pm}] < 0$, i.e., $\Delta > 1 - D$. We note that when $D \geqslant 1$ this is satisfied by any positive Δ. To summarize, the part of the first quadrant of the (ω_0, Δ) plane where the incoherent state is stable is defined by the conditions: $\Delta > 1 - D + \sqrt{1 - \omega_0^2}$ for $\omega_0 \leqslant 1$, and $\Delta > 1 - D$ for $\omega_0 > 1$. From what we have noted, when $D \geqslant 2$ these conditions define the whole first quadrant, and in that case the incoherent state is always stable. We will see in the following that, actually, for $D \geqslant 2$ the phase diagram is trivial, since the only stationary state is the incoherent state; thus, the interesting cases occur for $D < 2$.

To conclude the analysis of the stability of the incoherent state, we note that, although the system has infinite equations, the analysis can be performed exactly, since the linearization of the system around this state results in independent equations for $n \geqslant 2$, all of them associated to eigenvanlues with negative real part for any $D \geqslant 0$, while the two coupled equations for $n = 1$ can be easily studied. In particular, we note that the results obtained from the equations for $n = 1$ are analogous to those found for $D = 0$ [19], that are recovered by simply posing $D = 0$ in equation (32).

3.2. Reduced system of equations

Equations (22) and (23) admit other stationary solutions, in addition to the incoherent ones $r_n^{(1)} = r_n^{(2)} = 0$. In the noiseless $D = 0$ case the Ott–Antonsen ansatz allows to have a closed system involving just $r_1^{(1)}$ and $r_1^{(2)}$, and it is possible to perform an analytical evaluation of the stationary solutions. In our case we have an open system, and we have to resort to a numerical evaluation. This can be done by truncating the system to a given value of n, sufficiently large to represent with very good approximation the full infinite system. That this truncation is a feasible and meaningful approximation can be understood from the fact that it is expected that a stationary state will give rise to a distribution function $\rho(\theta, \omega)$ such that the modulus of the order parameters r_n decreases rapidly with n, since to have a finite value of r_n for large n requires a wildly fluctuating distribution function. Therefore, our numerical study of the system of equations has been performed by putting equal to 0 all the variables $r_n^{(1)}$ and $r_n^{(2)}$ for $n > M$, thus obtaining a closed system of $2M$ equations. We have chosen $M = 50$, and we have verified that in all cases our results for the main order parameter r_1 do not change by taking a larger value of M.

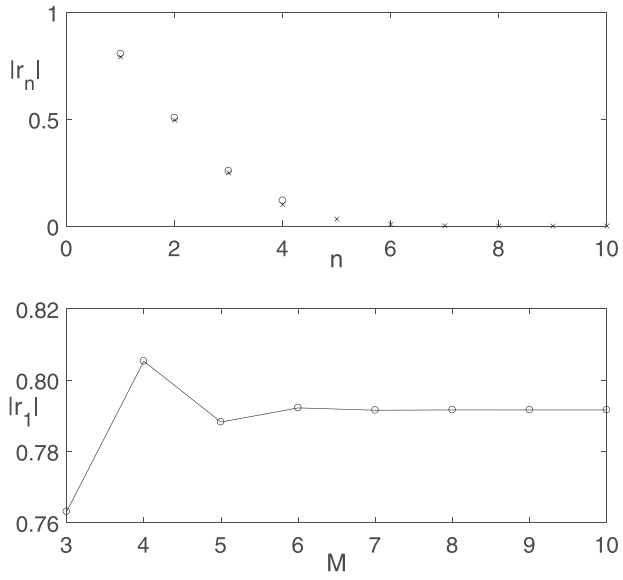

Figure 1. Upper panel: the value of $|r_n|$, where r_n is defined in equation (17), corresponding to the stationary state of the system of equations (22) and (23), as a function of n, for the parameters values $\Delta = 0.3$, $\omega_0 = 0.774$ and $D = 0.5$. The open circles have been obtained with the system cut at $M = 4$ (thus n can be at most equal to 4), while the crosses with the system cut at $M = 10$; for $M > 10$ the values are practially indistinguishable from those corresponding to $M = 10$. Lower panel: $|r_1|$ of the stationary state, for the same set of parameters, as a function of the cut value M; the line joining the points is just a guide to the eye.

It is useful, before proceeding with the analysis of the partially synchronized states, to provide a further argument and a numerical evidence to support the above claim about the possibility to cut the system at a not very large value of M. First, we recall the fact that for $D = 0$ the partially synchronized states are characterized by the equalities $r_n^{(1)} = \left[r_1^{(1)}\right]^n$ and $r_n^{(2)} = \left[r_1^{(2)}\right]^n$. This implies an exponential decay with n of the modulus of the parameters $r_n^{(1)}$ and $r_n^{(2)}$; this is easily seen by posing, e.g., $\alpha_j = -\ln r_1^{(j)}$, with $j = 1, 2$, so that $\mathrm{Re}\left[\alpha_j\right] > 0$, with the above equalities becoming $r_n^{(j)} = \exp\left[-n\alpha_j\right]$. The equalitites are no more satisfied when $D > 0$, but we can expect that, from the numerical point of view, something similar occurs. Then, if $r_n^{(1)}$ and $r_n^{(2)}$ decay so rapidly with n, it is very plausible that a system cut at a value of M which is not very large, posing $r_n^{(1)} = r_n^{(2)} = 0$ for $n > M$, will approximate extremely well the whole system. As a numerical evidence, in figure 1 we show two plots. For a representative set of values of the parameters Δ, ω_0 and D, the upper panel gives the value of the modulus of the stationary value of $r_n = \left(r_n^{(1)} + r_n^{(2)}\right)/2$ as a function of n as obtained from equations (22) and (23) cut at different values of M: the small open circles correspond to $M = 4$ (thus they stop at $n = 4$), while the crosses correspond to $M = 10$. The plot shows the rapid decay with n, and that, when the values are present for both values of M, they are very close. However, the most important point is that the values obtained for $M > 10$ are practically indistinguishable from those corresponding to $M = 10$, proving that such a small value of M already provides practically exact values. A further evidence, concerning r_1, is given in the lower panel of figure 1, where the stationary value of $|r_1|$ is plotted as a function of the cut

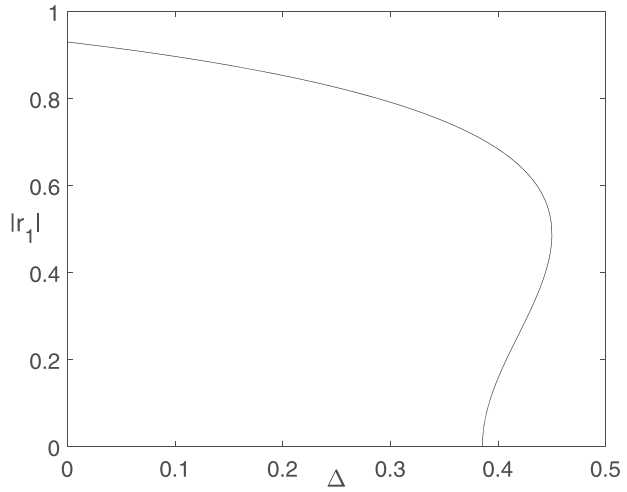

Figure 2. The order parameter $|r_1|$ corresponding to the stationary state of the system of equations (22) and (23) as a function of Δ for $D = 0.5$, with ω_0 constrained to be equal to 2.58Δ.

value M. After $M = 10$ this value is constant within machine precision. In conclusion, it is evident that a choice of $M = 50$ is more than plausible to obtain a precise value of the order parameters $r_1^{(1)}$ and $r_1^{(2)}$.

3.3. Partially sinchronized stationary states

In figure 2 we plot an example of the value of the modulus $|r_1|$ of the order parameter $r_1 = \frac{1}{2}(r_1^{(1)} + r_1^{(2)})$ corresponding to the stationary state of the system of equations (22) and (23). This quantity is plotted for the particular value $D = 0.5$ and as a function of Δ, with ω_0 constrained to be equal to 2.58Δ; practically, $|r_1|$ is given as a function of a quantity proportional to the distance from the origin in the first quadrant of the (ω_0, Δ), distance computed along the line $\omega_0 = 2.58\Delta$. There is no reason for the choice of a particular value of the latter proportionality constant, i.e. we could have chosen another proportionality constant γ such that $\omega_0 = \gamma\Delta$. We will return to this point shortly. At the transition point, that in figure 2 is at $\Delta \approx 0.385$, a stationary solution with positive $|r_1|$ bifurcates continuously from the incoherent solution $r_1 = 0$. In general this transition can be supercritical or subcritical. It is known [15] that for $D = 0$ the syncronization transition is supercritical for a symmetric unimodal frequency distribution $g(\omega)$, while it is subcritical for a symmetric bimodal distribution, in which the second derivative of $g(\omega)$ at $\omega = 0$ is positive. In the latter case we would have a plot qualitatively similar to the one in figure 2, with $|r_1|$ initially increasing from 0 for increasing Δ (i.e., with the curve starting towards the right), while in the former case the curve would start towards the left. For our form of $g(\omega)$ the bimodal case corresponds to $\omega_0 > \frac{\Delta}{\sqrt{3}}$. This picture holds also in the noisy case $D > 0$, but the discriminating value of ω_0, determining if the transition is supercritical or subcritical,depends on D. This value can be found using a power series expansion that gives the stationary value of r_1 as a function of the parameters of the distribution $g(\omega)$; one obtains an expression valid for $r_1 \to 0$, sufficient to see if the synchronization transition is supercritical or subcritical [17]. The general expressions give the critical value K_c of the coupling constant K where the synchronization transition occurs and the value of r_1

for K in the neighbourhood of K_c [17]; using our dimensionless parameters one finds, for the particular $g(\omega)$ given by equation (3), that, for given D, the synchronization transition occurs in the (ω_0, Δ) plane for

$$\omega_0^2 = 2(\Delta + D) - (\Delta + D)^2, \tag{33}$$

and that the transition is subcritical if together with this equality one has

$$\omega_0^2 > (\Delta + 2D)(\Delta + D)^2/(3\Delta + 4D). \tag{34}$$

Some comments on the study of the synchronization transition using the circular cumulants mentioned at the end of section 2.2, will be made in the conclusions. In the (ω_0, Δ) plane, expression (33) defines the circumference with center in $(\omega_0, \Delta) = (0, 1 - D)$ and radius equal to 1, the same circumference found in the study of the stability of the incoherent state. It should be now clear how to compute the value of γ such that, in a graph of $|r_1|$ vs Δ like that in figure 2, with ω_0 constrained to be equal to $\gamma\Delta$, the transition is subcritical: if equation (34) is taken as an equality, its right hand side is equal to that of equation (33), so that one obtains an equation that can be solved for Δ as a function of D; it is the value of Δ where the synchronization transition occurs at the boundary between supercriticality and subcriticality. Denoting this value of Δ with, e.g., Δ_D, from equation (33) we derive that the corresponding value γ_D is given by

$$\gamma_D = \frac{\sqrt{2\,(\Delta_D + D) - (\Delta_D + D)^2}}{\Delta_D}. \tag{35}$$

Thus, the transition is subcritical, and the plot of $|r_1|$ vs Δ is as in figure 2, when at the transition $\omega_0 > \gamma_D\Delta$, i.e., when in the plot ω_0 is constrained to be equal to $\gamma\Delta$ with $\gamma > \gamma_D$. In this case we see that, for the range of Δ between that of the transition and the one where the curve reaches its rightmost point, there are two stationary states with positive $|r_1|$ (beyond the one with $r_1 = 0$ which is always present). We expect that the one corresponding to the larger value of r_1 is stable, while the other is unstable, and this has been confirmed in all cases by the numerical results.

Finally, we note that it is easy to see that the ω_0 value of the transition, as given in equation (33), is always $\leqslant 1$, and that solved for Δ it gives $\Delta = 1 - D \pm \sqrt{1 - \omega_0^2}$; the solution with the positive sign before the square root coincides with the threshold for the stability of the incoherent state.

3.4. The structure of the phase diagram

The above analysis allows us to build a partial (but almost complete) structure of the phase diagram of the asymptotic states of the system. This phase diagram is plotted in figure 3 for $D = 0.5$, the same value used in figure 2. The structure will be completed in the next section after considering the standing wave states. We prefer to present at this point the picture of the phase diagram, to show its richness, since the further feature that will be introduced after the analysis in section 4 involves only a relatively small region of the diagram.

In the plot lowercase letters are used to denote the intersections of different full lines or of a full line with one coordinate axis or a boundary of the plot; roman numbers are used to denote the different regions delimited by these lines. We begin by explaining which are the asymptotic states that occur in the different regions of the diagram. Then we will proceed to a description

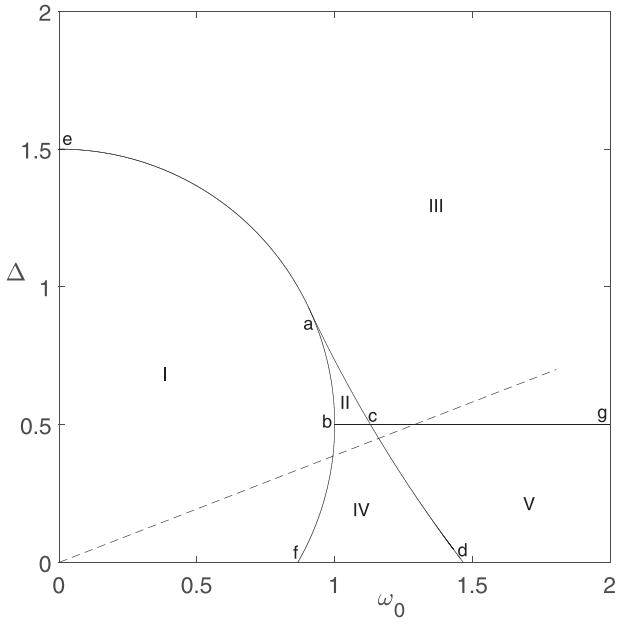

Figure 3. The partial structure of the phase diagram for $D = 0.5$. See the text for the description of the full lines, the meaning of the lowercase letters and roman numbers, and an explanation of the stability properties of the stationary states in the different regions of the diagram. The dashed line is the one along which the plot of $|r_1|$ vs Δ in figure 2 has been computed.

of the various lines and how they have been obtained on the basis of the analysis presented above.

The incoherent state $r_1 = 0$ is stable in regions II and III. On the other hand, the partially synchronized state exists and is stable in regions I, II and IV. Then, in the small region II both the incoherent state and the partially synchronized state are stable; the stationary asymtpotic state reached by the system depends on the initial condition. We have here the first example of bi-stability. Region V is the one where standing wave states occur. We will study these states in section 4, and we will complete the phase diagram for $D = 0.5$.

Let us now see how the lines delimiting the regions have been obtained. We begin by considering the lines '*eabf*' and '*bcg*'. The curved line '*eabf*' is the part of the circumference with center in $(\omega_0, \Delta) = (0, 1 - D) = (0, 0.5)$, and radius equal to 1, that lies in the first quadrant; the horizontal line '*bcg*', actually extending indefinitely for $\omega_0 > 1$, is at $\Delta = 1 - D = 0.5$. According to the analysis presented in section 3.1, after equation (32), the incoherent state $r_1 = 0$ is stable for $\Delta > 1 - D + \sqrt{1 - \omega_0^2}$ when $\omega_0 \leqslant 1$, and for $\Delta > 1 - D$ when $\omega_0 > 1$, i.e., in the part of the diagram which is, at the same time, outside the line '*eabf*' and above the horizontal line, '*bcg*'; namely, in regions II and III. We now consider the almost (but not quite) straight line '*acd*'. It is defined as the locus of (ω_0, Δ) points where the plots like the one on figure 2 reach their righmost point, each plot characterized by a different γ value larger than γ_D. The point '*a*', intersection of this line with the circumference, is the one where equation (34) is satisfied as an equality, in addition to equation (33). Then, from the analysis presented in section 3.3, one easily deduces that the partially synchronized state exists and is stable inside the circumference and in the part of the diagram outside the circumference but to the left of the

line '*acd*', i.e., in regions I, II and IV. As we have noted before, in the small region II, above the horizontal line and delimited by the circumference and the line '*acd*' (i.e., the region '*abc*'), both the incoherent state and the partially synchronized state are stable, giving an example of bi-stability.

We make the following remark concerning the appearance of the stationary solution with positive $|r_1|$, that bifurcates from the incoherent solution at the points defined by equation (33). If this transition is supercritical, the bifurcating solution is the only one with positive $|r_1|$, and it is stable, while the incoherent solution is stable up to the transition point; this occurs in the section '*ea*' of the circumference, with the incoherent solution stable outside the circumference and up to it, and the solution with positive $|r_1|$ existing and stable inside the circumference. On the other hand, when the transition is subcritical, as in the section '*abf*' of the circumference, at the transition the positive $|r_1|$ solution bifurcating from the incoherent one is unstable, and there is another partially synchronized state with larger $|r_1|$. As far as the stability of the incoherent state is concerned, we have seen above that it is stable outside and up to the circumference for $\Delta > 1 - D$, while it is already unstable, before reaching the circumference, for $\Delta < 1 - D$ (see also below, section 4.1).

Finally, we point out that the dashed line in figure 3 is the one along which the plot of $|r_1|$ vs Δ in figure 2 has been computed.

After studying the standing wave states in section 4 and completing the phase digram for $D = 0.5$, we will consider other ranges for the value of D, where the structure of the diagram changes. But for the moment, we treat some features related to the stability of the partially synchonized stationary states.

3.5. Stability properties

In all cases we have found that the partially synchronized stationary states are represented by stationary solutions of equations (22) and (23) where $|r_n^{(1)}| = |r_n^{(2)}|$, in particular $|r_1^{(1)}| = |r_1^{(2)}|$. This had to be expected on physical grounds, from the invariance of the frequency distribution $g(\omega)$ for $\omega \to -\omega$. The numerical solutions of equations (22) and (23) have shown that these aymptotic solutions are reached even when the initial conditions do not satisfy the above equalities. Although without any rigour, this should practically prove that there are not stationary states that do not satisfy the equalities.

In this section we study numerically the linear stability of the partially synchronized states, and for this purpose we use a modified version of the systems of equations. Precisely, we go from the variables $r_n^{(1)}$ and $r_n^{(2)}$ to the variables r_n already defined in equation (17) and new variables b_n:

$$r_n = \frac{1}{2}\left[r_n^{(1)} + r_n^{(2)}\right] \tag{36}$$

$$b_n = \frac{1}{2\mathrm{i}}\left[r_n^{(1)} - r_n^{(2)}\right]. \tag{37}$$

With these variables equations (22) and (23) are replaced by:

$$\dot{r}_n = -n\left(\Delta + nD\right) r_n - n\omega_0 b_n - 2n\left(r_1^* r_{n+1} - r_1 r_{n-1}\right) \tag{38}$$

$$\dot{b}_n = -n\left(\Delta + nD\right) b_n + n\omega_0 r_n - 2n\left(r_1^* b_{n+1} - r_1 b_{n-1}\right). \tag{39}$$

In the equations for $n = 1$ it is understood that $r_0 \equiv 1$ and $b_0 \equiv 0$. Like equations (22) and (23), these equations are invariant with respect to the transformation $r_n \to r_n \mathrm{e}^{-\mathrm{i}n\psi}$ and $b_n \to b_n \mathrm{e}^{-\mathrm{i}n\psi}$

for arbitrary ψ, due to the global rotational invariance of the system. The coefficients appearing in these equations are all real, and then it is possible to restrict the study to real solutions. From equations (36) and (37) we see that real solutions r_n and b_n require not only that $|r_n^{(1)}| = |r_n^{(2)}|$, but in addition also that $r_n^{(1)*} = r_n^{(2)}$. However, the transformations $r_n \to r_n e^{-in\psi}$ and $b_n \to b_n e^{-in\psi}$, that brings solutions into solutions, while spoiling the latter equality, conserves the former, that, as mentioned above, has always been found to be satisfied for the partially synchronized stationary states. This suggests to study the linear stability of the partially synchronized states in the following way (although the numerical results clearly show that these states are stable, it is useful to have an independent confirmation based on a linear stability analysis). We consider a real solution of equations (38) and (39) corresponding to such a state, and we linearize the equations with respect to this solution. Then we can study separately the real and the imaginary parts of the linearized equations.

Denoting $r_n(t) = r_n^0 + \delta r_n(t)$ and $b_n(t) = b_n^0 + \delta b_n(t)$, where r_n^0 and b_n^0 are the real stationary solutions, the linearized equations are:

$$\dot{\delta r}_n = -n\,(\Delta + nD)\,\delta r_n - n\omega_0 \delta b_n - 2n\left(\delta r_1^* r_{n+1}^0 + r_1^0 \delta r_{n+1} - \delta r_1 r_{n-1}^0 - r_1^0 \delta r_{n-1}\right) \tag{40}$$

$$\dot{\delta b}_n = -n\,(\Delta + nD)\,\delta b_n + n\omega_0 \delta r_n - 2n\left(\delta r_1^* b_{n+1}^0 + r_1^0 \delta b_{n+1} - \delta r_1 b_{n-1}^0 - r_1^0 \delta b_{n-1}\right). \tag{41}$$

Writing explicitly the real and the imaginary parts of the perturbations, $\delta r_n = \delta r_n^{\mathrm{R}} + \mathrm{i}\delta r_n^{\mathrm{I}}$ and $\delta b_n = \delta b_n^{\mathrm{R}} + \mathrm{i}\delta b_n^{\mathrm{I}}$, we obtain the two sets of equations:

$$\dot{\delta r}_n^{\mathrm{R}} = -n\,(\Delta + nD)\,\delta r_n^{\mathrm{R}} - n\omega_0 \delta b_n^{\mathrm{R}} - 2n\left(\delta r_1^{\mathrm{R}} r_{n+1}^0 + r_1^0 \delta r_{n+1}^{\mathrm{R}} - \delta r_1^{\mathrm{R}} r_{n-1}^0 - r_1^0 \delta r_{n-1}^{\mathrm{R}}\right) \tag{42}$$

$$\dot{\delta b}_n^{\mathrm{R}} = -n\,(\Delta + nD)\,\delta b_n^{\mathrm{R}} + n\omega_0 \delta r_n^{\mathrm{R}} - 2n\left(\delta r_1^{\mathrm{R}} b_{n+1}^0 + r_1^0 \delta b_{n+1}^{\mathrm{R}} - \delta r_1^{\mathrm{R}} b_{n-1}^0 - r_1^0 \delta b_{n-1}^{\mathrm{R}}\right) \tag{43}$$

for the real parts, and

$$\dot{\delta r}_n^{\mathrm{I}} = -n\,(\Delta + nD)\,\delta r_n^{\mathrm{I}} - n\omega_0 \delta b_n^{\mathrm{I}} - 2n\left(-\delta r_1^{\mathrm{I}} r_{n+1}^0 + r_1^0 \delta r_{n+1}^{\mathrm{I}} - \delta r_1^{\mathrm{I}} r_{n-1}^0 - r_1^0 \delta r_{n-1}^{\mathrm{I}}\right) \tag{44}$$

$$\dot{\delta b}_n^{\mathrm{I}} = -n\,(\Delta + nD)\,\delta b_n^{\mathrm{I}} + n\omega_0 \delta r_n^{\mathrm{I}} - 2n\left(-\delta r_1^{\mathrm{I}} b_{n+1}^0 + r_1^0 \delta b_{n+1}^{\mathrm{I}} - \delta r_1^{\mathrm{I}} b_{n-1}^0 - r_1^0 \delta b_{n-1}^{\mathrm{I}}\right) \tag{45}$$

for the imaginary parts. Note that the two systems differ only for the sign of one term in each equation. In a transformation $r_n \to r_n e^{-in\psi}$ and $b_n \to b_n e^{-in\psi}$ with infinitesimal $\delta\psi$ we have, at first order, $\delta r_n = -in\delta\psi r_n$ and $\delta b_n = -in\delta\psi b_n$. And actually we have found, for any real r_n^0 and b_n^0 corresponding to a stationary state, that the eigenvalues of the system (42) and (43) have all negative real parts, while the eigenvalues of the system (44) and (45) have all negative real parts except one vanishing eigenvalue, whose eigenvector is exactly of the form $\delta r_n = -n\delta\psi r_n^0$ and $\delta b_n = -n\delta\psi b_n^0$. This confirms the expected stability of the partially synchronized stationary state and the existence of a neutral perturbation corresponding to a global rotation of the system.

To provide a visualization of the behaviour of the eigenvalues, in figure 4 we show the eigenvalues (denoted with μ) of the system (42) and (43) (upper panel) and of the system (44) and (45) (lower panel) for a representative choice of the parameters. The main plots show both the real part (stars) and the imaginary part (pluses) of the first 14 eigenvalues, while the insets show the real part μ_{R} of all 100 eigenvalues (we remind that we have chosen $M = 50$). As remarked above, all the eigenvalues of the system (42) and (43) have a negative real part, while all the eigenvalues except the first one of the system (44) and (45) have a negative real part,

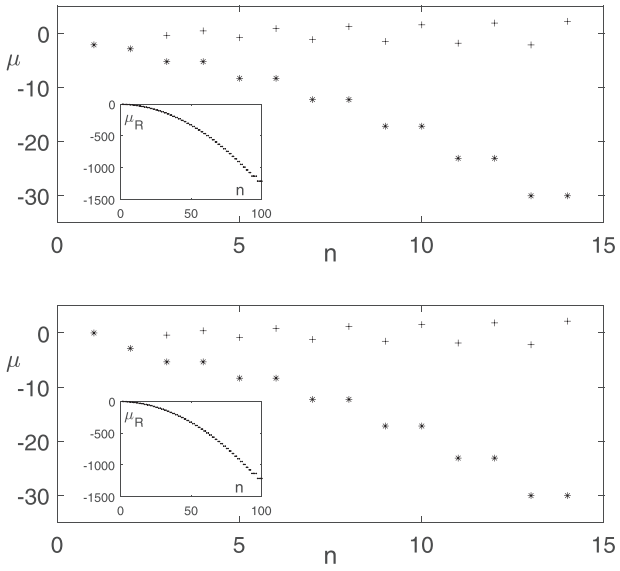

Figure 4. Eigenvalues of the system (42) and (43) (upper panel) and of the system (44) and (45) (lower panel), describing the linear dynamics around the partially synchronized state, having $|r_1| = 0.779$, of the model with $D = 0.5$, $\Delta = 0.448$ and $\omega_0 = 0.314$. In the main plots the stars and the pluses show the real and the imaginary part of the first 14 eigenvalues, respectively. The vanishing imaginary parts of the first two eigenvalues in both plots is not marked. The insets show the real part of all 100 eigenvalues.

that instead vanishes for the first one. In addition, for both systems the first two eigenvalues are real (and the corresponding vanishing imaginary part is not marked in the plots), while the others come in complex conjugate pairs; thus the first eigenvalue of the system (44) and (45) is equal to 0, this corresponding, as noted above, to the invariance of the system with respect to a global rotation.

4. The standing wave states and the full phase diagram

According to the above analysis, in the part of the diagram of figure 3 which is below the horizontal line and to the right of the line '*acd*', i.e., in region V, a partially sinchronized state does not exist, and the incoherent state is not stable. Nevertheless the system reaches an asymptotic state, that however is not a stationary state, but a periodic state, characterized by a limit cycle in the space of the order parameters r_n. For the noiseless $D = 0$ case, studied with the Ott–Antonsen ansatz, and with the assumption that $|r_1^{(1)}(t)| = |r_1^{(2)}(t)|$, one has a system of two equations [19]; it is then easy to recognize the appearance of a limit cycle in the 2D phase diagram. In our case the dimensionality of the dynamical phase space is, after the truncation, equal to $4M$ ($2M$ complex equations), in particular it is larger than 2, and therefore it is not possible to apply the Poincaré–Bendixson theorem. However, the periodic asymptotic states reached by the system are still to be recognized as limit cycles: they are subsets of low dimensionality in a high-dimensional space. It should be remarked that with the characterization of the dynamics with the circular cumulants [20–22], the low dimensionality of the limit cycle

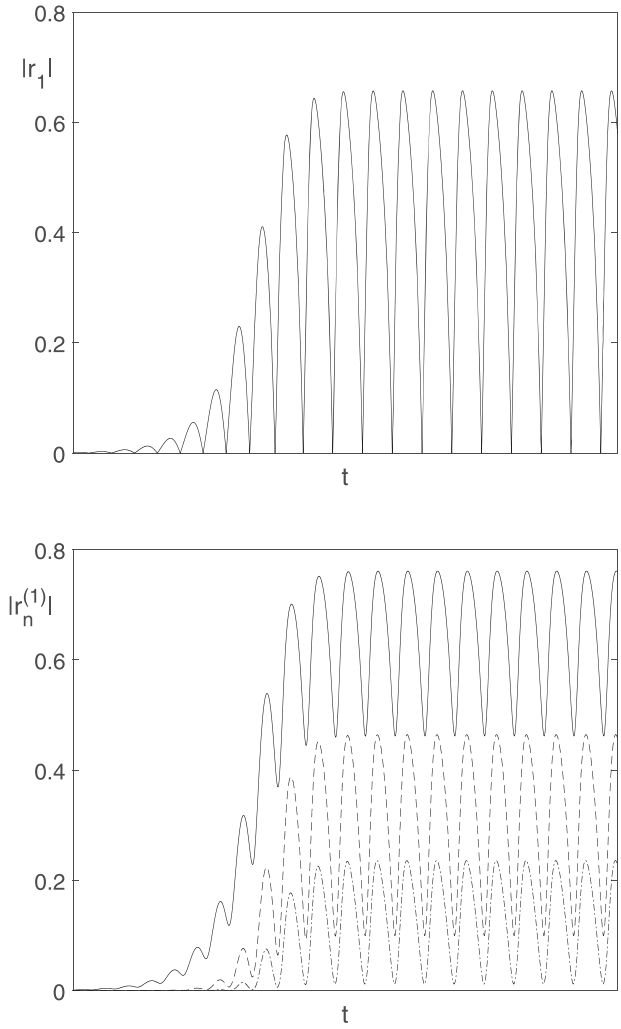

Figure 5. The dynamical evolution of $|r_1(t)|$ (upper panel) and of $|r_n^{(1)}(t)|$ for $n = 1, 2, 3$ (lower panel) as obtained from the solution of the system of equations (22) and (23) in a case in which the asymptotic state is a standing wave. In the lower panel the full line, the dashed line and the dash-dotted line refer, respectively, to $n = 1$, $n = 2$ and $n = 3$. Once the asymptotic periodic state is reached, the equalities $|r_n^{(1)}(t)| = |r_n^{(2)}(t)|$ are satisfied. Time is in arbitrary units.

could appear more evident, especially at low noise, when, loosely speaking, the 'deviation' of the dynamics from the manifold defined by the Ott–Antonsen ansatsz is expected to be small (see the last paragraph of section 2.2).

In the noiseless system the limit cycle is identified with the propagation of a standing wave [19]. In our case, the identification requires more care; it can be established with the following. We have verified that in a periodic asymptotic state the equalitites $|r_n^{(1)}(t)| = |r_n^{(2)}(t)|$ are satisfied for each n, and that all $|r_n^{(j)}(t)|$ ($j = 1, 2$) and all $|r_n(t)|$ vary periodically with the same period. An example is provided in figure 5, in which we plot $|r_1(t)|$ (upper panel) and $|r_n^{(1)}(t)|$ for $n = 1, 2, 3$ (lower panel), as obtained from the solution of the system of equations (22)

and (23) in a case in which the asymptotic state is a limit cycle. Such asymptotic states, where the modulus of all the order parameters (10) vary periodically with the same period, can clearly be seen as a standing wave propagating through the system.

We note that a periodic state, corresponding to the propagation of a standing wave in the system, appears to be physically very reasonable. While the partial synchronization of a stationary state is realized when a macroscopic fraction of oscillators is entrained at $\omega = 0$,[4] with the remaining oscillators drifting, one can argue that a standing wave state is realized when there are two macroscopic fractions, each one entrained at a frequency close to that of one of the two peaks of $g(\omega)$, with the remaining oscillators drifting. By the symmetry of $g(\omega)$, it is expected that the two entraining frequencies are symmetric with respect to $\omega = 0$, and that the two macroscopic fractions are equally populated. Then, the two groups of entrained oscillators rotate in opposite directions. It should be now clear what happens: focusing e.g. on the main order parameter ($n = 1$), we see that $r_1^{(1)}(t)$ and $r_1^{(2)}(t)$, while satisfying $|r_1^{(1)}(t)| = |r_1^{(2)}(t)|$ at any t, rotate in opposite directions with nonconstant angular velocities that are, at any t, equal in magnitude. When the angle between the two quantities in the complex plane is equal to π, i.e., when $r_1^{(1)}(t) = -r_1^{(2)}(t)$, then $r_1(t) = r_1^{(1)}(t) + r_2^{(2)}(t) = 0$, and this explains why in the standing wave state $|r_1(t)|$ reaches the value zero.

A study of the linear stability of the standing wave would require a Floquet analysis of the periodic solution of the system of equations. We have not performed this analysis, and we therefore limit ourselves to the numerical evidence of the stability of such states.

Actually, it happens that standing wave states, that we remind are found as the only asymptotic states in region V, occur also in part of region IV, where the incoherent state is unstable. This region is delimited by another line, the one denoted by '*bh*', as shown in figure 6. This plot gives the complete phase diagram for $D = 0.5$. Comparing with figure 3 we note that part of the region denoted by IV in that figure, now constitutes the new region denoted by VI. In the new region VI both the partially synchronized state and the standing wave state are stable, the one reached as the asymptotic state depending on the initial conditions. We have here the other example of bi-stability.

4.1. Classification of bifurcations

Referring to figure 6, we give a brief description of the type of bifurcations associated to the passage, crossing the lines in the diagram, from one kind of asymptotic state to another. A very vivid explanation of the various types of bifurcation can be found in [27].

Let us begin with the transition associated to the crossing of the circumference '*eabf*'. We have seen that at this crossing a stationary state with positive $|r_1|$ bifurcates from the always existing incoherent stationary state with $r_1 = 0$. In the section '*ea*' of the circumference the bifurcating positive $|r_1|$ state exists only inside the circumference, while in the section '*abf*' it exists only outside the circumference. This is the characteristic of a pitchfork bifurcation, with one of the stationary states existing only on one side of the transition. Actually, such bifurcation is in general associated with dynamical systems with symmetry, with two symmetric bifurcating states; in this case, $|r_1|$ is defined to be nonnegative, and the symmetric state does not exist. In the supercritical case (section '*ea*') the bifurcating solution is stable, while in the

[4] A perfect locking of frequencies can be realized in noiseless systems, but for noisy systems such perfect situations cannot occur, and phase slips are always present, although they might be quite rare [1]. For this reason it is preferable to talk about entrainment of oscillators.

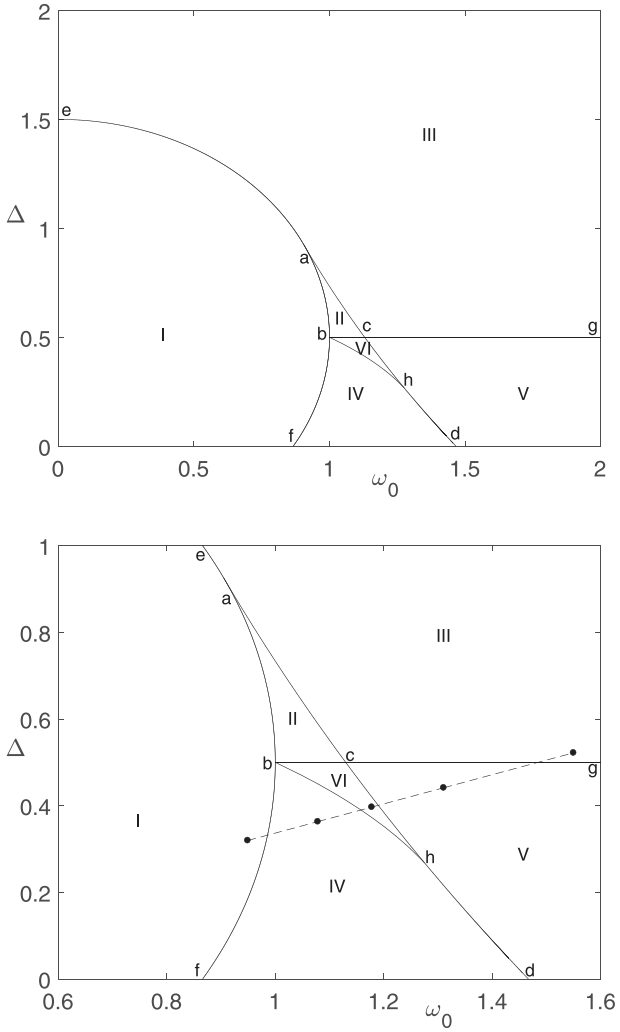

Figure 6. The full phase diagram for $D = 0.5$. The lower panel is a zoom of the more interesting region. As explained in the text, regions II and VI are characterized by the coexistence of two different asymptotic states; which one is reached by the system depends on the initial conditions. In region II both a stable incoherent state and a stable partially synchronized state are possible, while in region VI one can have either a stable partially synchronized state or a stable standing wave state. The full dots of the dashed line denote the points interested in the numerical simulation of the full oscillators system (see section 6).

subcritical case (section '*abf*') the bifurcating solution is unstable. In section '*bf*' the incoherent state is unstable on both sides of this transition (contrary to the canonical case of a pitchfork bifurcation); this is because it looses stability before, but this does not change the nature of this bifurcation.

We now consider the straight line '*bcg*'. Crossing this line from above, the incoherent state looses stability, with the creation of a stable limit cycle, the standing wave state. This is the typical case of a supercritical Hopf bifurcation. In section '*bc*' of the line a stable partially

synchronized state with finite $|r_1|$ already exists at the transition, together with the incoherent state, while in section '*cg*' the only stable state before the transition is the incoherent one.

Crossing the line '*achd*' from the right, we have the appearance of two stable partially synchronized states with finite $|r_1|$, one stable and the other unstable. We consider separately the section '*ach*' and the section '*hd*'. In the former case we have a saddle-node bifurcation; the other stable state, i.e., the incoherent $r_1 = 0$ state in section '*ac*', or the stable standing wave state in section '*ch*', does not take part in the bifurcation. On the orther hand, in section '*hd*', crossing the line from the right we have the disappearance of a stable limit cycle and the appearance of the two partially synchronized states, one stable and the other unstable. Here we have a saddle-node infinite period bifurcation, in which the period of the limit cycle tends to infinite at the bifurcation, i.e., it develops a fixed point, that after the transition splits in the two partially synchronized states, the node and the saddle.

Finally, we consider the line '*bh*'. Crossing this line from the right, the limit cycle, i.e., the standing wave state, disappears. This is a homoclinic bifurcation, in which the limit cycle, at the transition, reaches the saddle at $r_1 = 0$, with the appearance of a homoclinic orbit. After the transition this orbit disappears, leaving the saddle at $r_1 = 0$. The partially synchronized state exists throughout the transition and does not take part in it.

5. Larger values of D

Having completed the analysis of the phase diagram for $D = 0.5$, we now study how the structure of the diagram changes when D is varied. But first let us make a comparison with the phase diagram for $D = 0$, analyzed in [19]. As remarked above, the Ott–Antonsen ansatz, applicable when $D = 0$, allows to have a closed four-dimensional dynamical system, reduced to two dimensions with further assumptions, something which is not possible for positive D. In spite of this, we find that the phase diagrams for $D = 0$ and $D = 0.5$ are qualitatively the same, and also the type of bifurcations are the same. We note in particular that the circumference '*eabf*' and the line '*bcg*' are linearly shifted downward with D, as one can see from expression (33) defining the circumference and expression (32) giving the stability thresholds for the incoherent state: the center of the circumference is placed in $(\omega_0, \Delta) = (0, 1 - D)$, and the real part of the eigenvalue determining stability for $\omega_0 > 1$ is $1 - D - \Delta$. On the other hand, the other lines of the phase diagram, i.e., '*achd*' and '*bh*', do not share this exact property. For example, while points '*a*' and '*h*' have coordinates $(\sqrt{3}/2, 3/2)$ and about $(1.359, 0.748)$, respectively, for $D = 0$ [19], their coordinates for $D = 0.5$ are $(0.905, 0.925)$ and $(1.275, 0.269)$, respectively; then, the coordinates for $D = 0.5$ are not obtained by those for $D = 0$ with a $(0, -0.5)$ shift, but the difference is not large.

As a consequence of the above considerations, we expect that by increasing D the structure of the phase diagram will shift downward in the (ω_0, Δ) plane. The first qualitative change will occur when point '*h*' reaches the ω_0 axis. We have found that this occurs for $D \approx 0.765$. Then, in figure 7 we plot the phase diagram for $D = 0.9$. Since by now the overall structure of the diagram is clear, we plot directly a zoom of the interesting region, that includes all the transition lines. The main difference with respect to the phase diagram for $D = 0.5$ is that the line '*bh*' reaches the ω_0 axis before reaching the line '*acd*' of the saddle-node transition. As a consequence, the diagram does not present any more the section '*hd*' of the transition line that is found in figure 6, and the corresponding saddle-node infinite period bifurcation. Thus, it is no more possible to have a direct transition from region V to region IV, but only passing through region VI: the partially synchronized state will always appear before the standing wave state disappears.

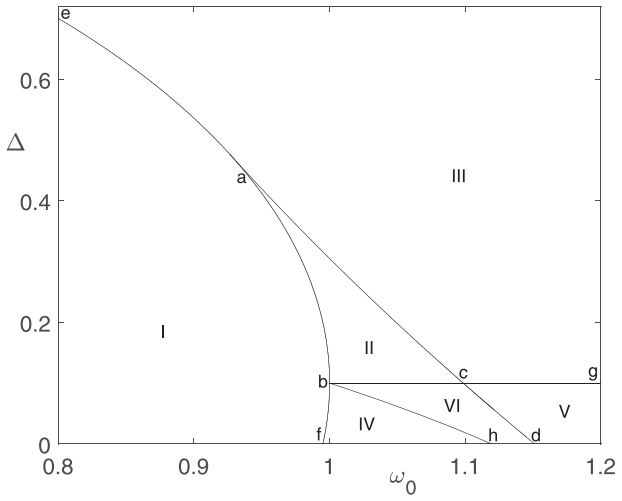

Figure 7. The interesting region of the phase diagram for $D = 0.9$. The meaning of the lowercase letters and roman numbers, is the same as in the diagram for $D = 0.5$ Also the stationary states or standing wave states are the same in the respective zones. The difference is that the line '*bh*' of the homoclinic bifurcation reaches the ω_0 axis before reaching the line '*acd*' of the saddle-node bifurcation.

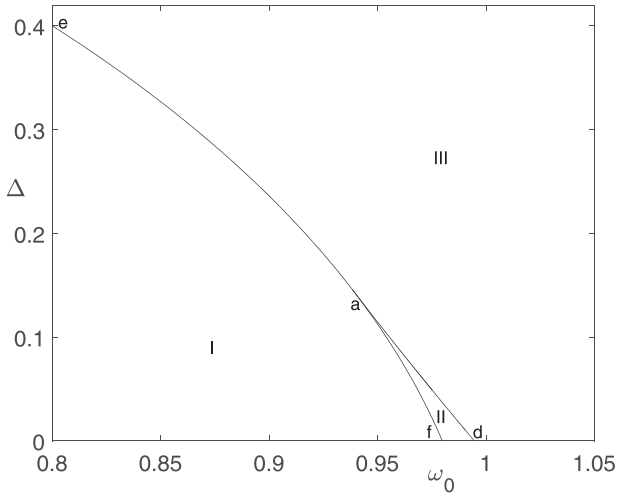

Figure 8. The interesting region of the phase diagram for $D = 1.2$. Only regions I, II and III are left, while the standing wave states, the Hopf bifurcation and the homoclinic bifurcation have disappeared.

By increasing D beyond $D = 1$ the line '*bcg*' of the Hopf bifurcation disappears, together with regions IV, V and VI, and the standing wave states. In figure 8 we plot the phase diagram for $D = 1.2$. With respect to the phase diagram for $D = 0.9$, regions IV, V and VI have disappeared. There are no more limit cycles corresponding to standing wave states, and the Hopf bifurcation and the homoclinic bifurcation do not occur any more. Only in region II

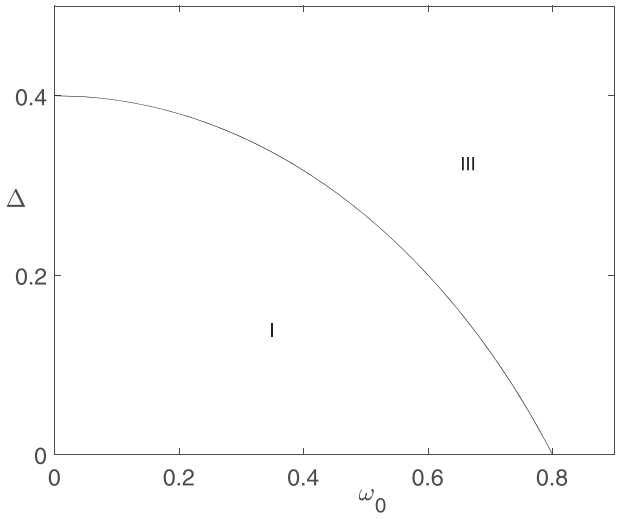

Figure 9. The phase diagram for $D = 1.6$. Only regions I and III, with a supercritical bifurcation between the incoherent state and the partially synchronized state, are left. This is the same simple situation that occurs, with or without noise D, with a unimodal frequency distribution.

we can now find the coexistence of two stationary states, the incoherent state and a partially synchronized state.

It is possible to find analytically up to which value of D the point 'a' exists. This threshold value is the one for which equations (33) and (34) considered as an equality have $\Delta = 0$ as solution. This occurs for $D = 4/3$. Beyond this value the only feature of the phase diagram is the arc of circumference with radius 1 and center in $(0, 1 - D)$ lying in the first quadrant. Clearly, we must also have $D < 2$, otherwise there is no such arc in the first quadrant. In figure 9 we plot the phase diagram for $D = 1.6$. Now there are only regions I and III, where, respectively, we have the partially synchronized stationary state and the incoherent stationary state. Crossing the transition line there is a supercritical bifurcation, corresponding to the transition between these two states. This is what is found in the case of a symmetrical unimodal frequency distribution, independently from the value of D. Physically, this can be understood from the fact that a large noise tends to mask the valley between the two peaks of the bimodal frequency distribution.

For $D > 2$ no transition lines are any more present, and the only stationary state is the incoherent one.

6. Numerical simulation of the dynamics

We have performed numerical simulations of the Langevin equations of the full system of coupled oscillators, equations (1), that have shown that the dynamics of the order parameters is well represented by the system of equations (22) and (23) truncated at a relatively small value of n. We will comment on this in the discussion, while in this section we focus on the observation of hysteresis. In fact, the presence of regions, in the parameter space, where different asymptotic states can exist, with the system choosing one of them depending on the initial conditions, makes it possible the existence of hysteresis.

In this section, since we have to refer to the original system parameters ω_0, Δ, D and K, we reintroduce the use of the hat for the reduced variables, that have been used throughout the paper, in particular in the plots of the phase diagram.

We have performed a simulation of equations (1) with 100 000 oscillators, with frequencies distributed according to equation (3) with $\omega_0 = 2.9696$ and $\Delta = 1$. Our purpose has been to simulate a dynamics where at predetermined times the coupling K is changed. In particular, we have started with a low value of K, for which the system is expected to reach an incoherent stationary state[5], and then we have increased K several times at predetermined times; after reaching a maximum value of K, we have reversed the process, going back to the same values of K up to the initial value. The points of the dashed line in the lower panel of figure 6 refer to this simulation. We have started the simulation with the system in the rightmost point of that line, denoted by a full dot, that belongs to region III; after a given time we have changed K so that to stay in the point of the dashed line inside region V; then another change of K has taken the system in the point of the dashed line inside region VI; and so on, we have then visited the point in region IV and the one in region I corresponding to the leftmost point of the dashed line. Then, we have reversed the changes of K, going back to the point in region III.

The phase diagram of figure 6 is at constant $\widehat{D} = 0.5$, therefore to simulate a system with given system parameters ω_0 and Δ, but with constant reduced noise $\widehat{D}$, at each variation of K we had to change correspondingly the value of D, since $\widehat{D} = \frac{4}{K}D$. The analogous relations for the other parameters, i.e. $\widehat{\omega_0} = \frac{4}{K}\omega_0$ and $\widehat{\Delta} = \frac{4}{K}\Delta$, give the variation of $\widehat{\omega_0}$ and of $\widehat{\Delta}$ when K is varied, and then determine how one moves on the phase diagram.

In figure 10 we plot the behaviour of the order parameter $|r_1|$ during the simulation. At the beginning, when the system is in region III, the order parameter is almost 0; of course it cannot be exactly 0, due to finite size effects, that are responsible for the fluctuations also in the following phases of the run. When the coupling K is increased so that the system is inside region V, we see that the dynamics enters a phase with an almost periodic variation of the order parameter. Again, the imperfect periodicity is caused by finite size effects; however, it is nice to see that the minimum value of $|r_1|$ during the oscillations is practically 0, as predicted by the reduced system of equations. A further increas of K, that brings the system in region VI, has the effect of enhancing the amplitude of the periodic variation of $|r_1|$. In this region, we had found the coexistence, together with the standing wave state, of a partially synchronized state; this is observed later in the simulation, marking the hysteresis of the dynamics. A further increase of K brings the system in region IV, and then in region I; this corresponds to the order parameter staying in a stationary value, corresponding to a partially synchronized state. When the reversed process is begun, going back to region IV, the previous value of $|r_1|$ is obtained, as shown in figure 10. However, when we now bring back the system in region VI, it settles to the partially synchronized state, although with fluctuations of $|r_1|$ somewhat larger than in regions I and IV; this can also be due to the fact that region VI is rather narrow, so that the values of the parameters are not very far from those at the boundary of the region. Taken back to region V, the system goes back to the only existing asymptotic state, the standing wave state, while brought back finally in region III, $|r_1|$ goes back to 0.

Summarizing, in the above dynamics the system is found twice in region VI, where different asymptotic states exist. The fact that in the first passage in the region the system settles in the

[5] Obviously for the full system stationarity refers to the value of the order parameter, not to the dynamical degrees of freedom.

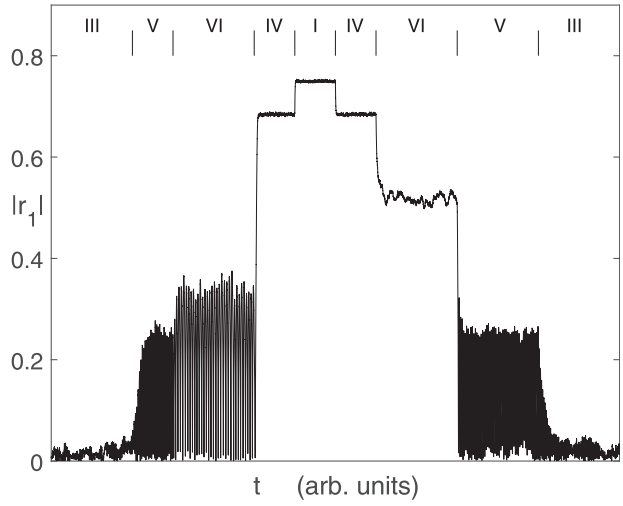

Figure 10. The order paramete $|r_1|$ as a function of time in a numerical simulation of equations (1), with 100 000 oscillators. The small vertical bars at the top of the plot denote the times in which the coupling K has been changed. The roman numbers show the region of the phase diagram in which the system parameters are located during that lapse of time; more precisely, the parameters of the system are those corresponding to the respective point of the dashed line in the lower panel of figure 6. The time lapses are not all equal.

periodic state, while in the second passage it goes to the stationary partially synchronized state, proves the existence of hysteresis loops.

7. Discussion and conclusions

The peculiarity of the frequency distribution used in this work, equation (3), is the fact that, when analytically continued to the complex ω plane, it has few poles. Of course it is not difficult to envisage other frequency distributions with the same property. We have seen that, even without the possibility of using the Ott–Antonsen ansatz, this gives the possibility to study directly the dynamics of the order parameter of the system, the main variable related to the synchronization transition. In a noiseless system the ansatz and the mentioned property of the frequency distribution allow, together, to reduce the study to a low dimensional system of equations, while in a noisy system the system of equations is still infinite dimensional, in principle. However, the dynamical variables of this system, equations (22) and (23), are the order parameters $r_n^{(1)}$ and $r_n^{(2)}$, and we have argued that at increasing n these variables approach rapidly zero, since a finite r_n for large n would require a distribution function with very large fluctuations (of course, one could study the Fokker–Planck equation (7) with such a distribution as initial condition, but in this case we expect, on physical grounds, that the fluctuations will smooth out rapidly). This allows to truncate the system at a reasonable small value (we have chosen $M = 50$ as the largest value of n), without spoiling the resulting dynamics.

We have found that at small values of the reduced noise parameter D the phase diagram of the system is qualitatively similar to that of the noiseless $D = 0$ case. The main quantitative difference is an approximate overall downward shift (i.e., an approximate translation in a

direction parallel to the Δ axis) of the transition lines, the overall shift quantified by the noise D itself. This downward shift is exact for the transition lines corresponding to the pithfork bifurcation and the Hopf bifurcation, while it is only approximate for the transition lines corresponding to the saddle-node bifurcation and the homoclinic bifurcation (for example, point 'a' reaches the $\Delta = 0$ axis for $D = 4/3$, but at $D = 0$ it is found at $\Delta = 3/2$ [19]).

The progressive simplification of the phase diagram at increasing values of D can be understood on physical grounds. We know that for a symmetric unimodal frequency distribution the only transition is the one between the incoherent state and the partially synchronized state, and that as soon as the latter exists, on one side of the (supercritical) transition, the former looses stability. This picture is independent on the level of noise, that determines only the location of the transition. A large noise can be physically interpreted as un uncertainty in the proper frequency of each oscillator, and then as a blurring of the frequency distribution (as we have remarked in the introduction, one main motivation for the introduction of noise in a system of coupled driven oscillators is the possibility to represent in this way the uncertainty and the fluctuations of the proper frequencies). This process tends to decrease the depth of the valley between the two peaks of a bimodal distribution, until the valley is completely washed out at large enough noise, and the system behaves as if it had a unimodal distribution.

We would like to comment on the relation of our work with the method developed in [20–22], where the circular cumulants have been introduced. As mentioned before, in that approach the dynamical variables $r_n^{(1)}$ and $r_n^{(2)}$ would be replaced by variables $\varkappa_n^{(1)}$ and $\varkappa_n^{(2)}$, and correspondingly one would obtain another system of equations, replacing equations (22) and (23). For each $j = 1, 2$, $\varkappa^{(j)}$ would be expressed as a function of $r_1^{(j)}, r_2^{(j)}, \ldots, r_n^{(j)}$. Full details can be found in the cited references. The main characteristic of these variables is that they make more transparent the limit to the manifold defined by the Ott–Antonsen ansatz, that as we know is invariant in the noiseless case. In fact the relations $r_n^{(j)} = \left[r_1^{(j)}\right]^n$ are translated in $\varkappa_n^{(j)} = 0$ for all $n \geqslant 2$.[6] The price to pay in the structure of the dynamical equations is that, for each $j = 1, 2$, the nth equation depends on all the dynamical variables $\varkappa_m^{(j)}$ with $m = 1, 2, \ldots, n+1$, and not only on those with $m = n-1, n, n+1$. On the other hand, there can be other advantages in the cumulant approach. For example, the fact that the manifold defined by the Ott–Antonsen ansatz is defined by $\varkappa_n^{(1)} = \varkappa_n^{(2)} = 0$ for $n \geqslant 2$ would allow to perform a perturbative analysis by keeping only the first few circular cumulants. On a more practical side, it is to be expected that the dynamical evolution would be approximated quite well by the first few cumulants, probably keeping only $n = 1$ and $n = 2$. We remark, though, that numerically also the dynamics approximated by the first several $r_n^{(1)}$ and $r_n^{(2)}$ (i.e., choosing a value of M much smaller than the value of 50 used in this work), is expected to be quite good in most cases, as one can argue, e.g., from figure 1. Another example is provided by the supercritical or subcritical nature of the pithcfork and Hopf bifurcations,that could be seen more directly: similarly to the case of small noise, the first two cumulants could provide a description of the dynamics in the neighbourhood of the bifurcation, where the modulus of the order parameter, $|r_1|$, is very small. Then, a study of the coefficients of this reduced system would reveal the nature of the bifurcation. In our case, one would see that the Hopf bifurcation is always supercritical, while it could be seen when the small $|r_1|$ solution bifurcating from the

[6] This is similar, e.g., to the passage from moments to cumulants in the characterization of probability distributions. In the case of a Gaussian distribution the relations between the moments are translated in the vanishing of all cumulants of order larger than 2

incoherent state in the pitchfork bifurcation is stable (supercritical case) or unstable (subcritical case).

A natural question that arises is what happens if the frequency distribution does not have the property of having just few poles when analitycally prolongued in the complex plane. In that case, the restriction of the dynamics to that of the order parameters, and practically to the first several r_n (or first several circular cumulants), is not possible, and one should analyze the full Fokker–Planck equation (7). Again we can try to resort to a physical argument. A frequency distribution made of, e.g., the sum of two Gaussians centered in $\pm\omega_0$, has an essential singularity at the point at infinity in the complex plane, and a study analogous to that in this work cannot be performed. However, it is possible to approximate numerically such a distribution with one decaying algebraically; the approximation would fail only at large frequencies, that will be the proper frequencies of few outlier oscillators. One can argue that these two systems should behave very similarly, presenting the same types of stationary or periodic asymptotic state, and the same types of transitions between them, with just small differences in the location of the transitions. The consequence of this argument is that, apart from numerical details, one could study the behaviour of a general system by trying to approximate as close as possible the frequency distribution with an algebraic one. Under this perspective, it is not by chance that for the noiseless system the numerical results for a sum of two Gaussians are close to those of the sum of two Lorentzians [19].

Adopting this point of view, it would be interesting to perform an analysis like the one presented in this work for more general frequency distributions $g(\omega)$, although still with the property of having few poles in the analytical continuation, and more general forms of the interaction between the oscillators. This could allow the study of the complete phase diagram, that could be even richer than the one occuring for symmetrical bimodal distributions. For example, the interaction given in equation (1), i.e., the interaction used in the Kuramoto model, is the simplest one if one considers the Fourier expansion of a generic interaction $h(\theta_i - \theta_j)$. This will have, in general, all the Fourier terms proportional to $\sin[k(\theta_i - \theta_j)]$ for each integer k (the terms proportional to the cosines are excluded if we want interactions derived from a potential). It has been found that noiseless $D = 0$ systems with this generic interaction have an order parameter that scales differently, with respect to the Kuramoto model, near the onset of the synchronization transition [25, 26]. Extension to the noisy case with generic interactions has shown that in this scaling behaviour there is a crossover, since the scaling tends to go back to the Kuramoto result when the noise strength increases [28, 29]. The study of the full phase diagram, at various noise strengths, could be very rewarding. On the other hand, restricting to the simple sine interaction, but considering nonsymmetrical frequency distributions, should give rise to new asymptotic states, like travelling waves. It would be equally interesting to study the effect of noise in this case, to see, e.g., what would be the effect of the blurring of the frequency distribution at large noise.

Acknowledgments

The author acknowledges financial support from INFN (Istituto Nazionale di Fisica Nucleare) through the projects DYNSYSMATH and ENESMA.

ORCID iDs

Alessandro Campa https://orcid.org/0000-0002-7182-7094

References

[1] Pikovsky A, Rosenblum M and Kurths J 2001 *Synchronization: A Universal Concept in Nonlinear Sciences* (Cambridge: Cambridge University Press)
[2] Buck J 1988 *Q. Rev. Biol.* **63** 265
[3] Wiesenfeld K, Colet P and Strogatz S H 1998 *Phys. Rev.* E **57** 1563
[4] Winfree A T 1980 *The Geometry of Biological Time* (New York: Springer)
[5] Bier M, Bakker B M and Westerhoff H V 2000 *Biophys.* J **78** 1087
[6] Filatrella G, Nielsen A H and Pedersen N F 2008 *Eur. Phys. J.* B **61** 485
[7] Ha S Y, Jeong E and Kang M J 2010 *Nonlinearity* **23** 3139
[8] Strogatz S H 2003 *Sync: The Emerging Science of Spontaneous Order* (New York: Hyperion)
[9] Kuramoto Y 1975 *International Symposium on Mathematical Problems in Theoretical Physics* (Lecture Notes in Physics vol 39) ed H Arakai (New York: Springer) p 420
[10] Kuramoto Y 1984 *Chemical Oscillations, Waves and Turbulence* (Berlin: Springer)
[11] Sakaguchi H 1988 *Prog. Theor. Phys.* **79** 39
[12] Ermentrout B 1991 *J. Math. Biol.* **29** 571
[13] Acebrón J A, Bonilla L L and Spigler R 2000 *Phys. Rev.* E **62** 3437
[14] Gupta S, Campa A and Ruffo S 2014 *Phys. Rev.* E **89** 022123
[15] Strogatz S H 2000 *Physica* D **143** 1
[16] Gupta S, Campa A and Ruffo S 2014 *J. Stat. Mech.: Theory. Exp.* R08001
[17] Gupta S, Campa A and Ruffo S 2018 *Statistical Physics of Synchronization* (Berlin: Springer)
[18] Ott E and Antonsen T M 2008 *Chaos* **18** 037113
[19] Martens E A, Barreto E, Strogatz S H, Ott E, So P and Antonsen T M 2009 *Phys. Rev.* E **79** 026204
[20] Tyulkina I V, Goldobin D S, Klimenko L S and Pikovsky A 2018 *Phys. Rev. Lett.* **120** 264101
[21] Goldobin D S, Tyulkina I V, Klimenko L S and Pikovsky A 2018 *Chaos* **28** 101101
[22] Goldobin D S and Dolmatva A V 2019 *Phys. Rev. Research* **1** 033139
[23] Daido H 1992 *Prog. Theor. Phys.* **88** 1213
[24] Daido H 1993 *Prog. Theor. Phys.* **89** 929
[25] Daido H 1994 *Phys. Rev. Lett.* **73** 760
[26] Daido H 1996 *Physica* D **91** 24
[27] Strogatz S H 1994 *Nonlinear Dynamics and Chaos* (Reading, MA: Perseus)
[28] Crawford J D 1995 *Phys. Rev. Lett.* **74** 4341
[29] Crawford J D and Davies K T R 1999 *Physica* D **125** 1